Magnetic Resonance Imaging 34 (2016) 980–989

Contents lists available at ScienceDirect

Magnetic Resonance Imaging

journal homepage: www.mrijournal.com

Original contribution

Morphological asymmetries of mouse brain assessed by geometric morphometric analysis of MRI data

Jimena Barbeito-Andrés [a,*], Valeria Bernal [b], Paula N. Gonzalez [a]

[a] IGEVET - Instituto de Genética Veterinaria 'Ing. Fernando N. Dulout' (UNLP-CONICET LA PLATA), Facultad de Cs. Veterinarias UNLP, La Plata, Buenos Aires, Argentina
[b] División Antropología, Facultad de Ciencias Naturales y Museo, Universidad Nacional de La Plata, CONICET, La Plata, Buenos Aires, Argentina

ARTICLE INFO

Article history:
Received 7 March 2016
Accepted 17 April 2016

Keywords:
MicroMRI
Landmarks and semilandmarks
Procrustes ANOVA
Shape asymmetry
Hippocampus

ABSTRACT

Mammalian brain has repeated structures at both sides of the median plane, although some asymmetries have been described even under normal conditions. Characterizing normal patterns of asymmetry in mouse brain is important to recognize features that depart from expected ranges in the most widely used mammalian model. Analyses on brain morphology based on magnetic resonance image (MRI) have largely focused on volumes while less is known about shape asymmetry. We introduce a flexible protocol based on geometric morphometrics to assess patterns of asymmetry in shape and size of mouse brain from microMRI scans. After systematic digitization of landmarks and semilandmarks, we combine multivariate methods for statistical analyses with visualization tools to display the results. No preliminary treatment of the images (e.g. space normalization) is needed to collect data on MRI slices and visual representations improve the interpretation of the results. Results indicated that the protocol is highly repeatable. Asymmetry was more evident for shape than for size. Particularly, fluctuating asymmetry accounted for more variation than directional asymmetry in all brain regions. Since this approach can detect subtle shape variation between sides, it is a promising methodology to explore morphological changes in the brain of model organisms and can be applied in future studies addressing the effect of genetic and environmental factors on brain morphology.

1. Introduction

Anatomical asymmetries across the sagittal plane in cortical and subcortical regions are a conserved feature of the mammalian brain [1]. Such structural differences between left and right sides of the brain, as well as functional bilateral specializations, originate in the normal course of individual ontogeny under the regulation of several factors, ranging from genetic and physiological to environmental ones [2,3]. In humans, the patterns of macrostructural brain asymmetry have been well studied mainly in relation to behavioral outputs, such as language and handedness, as well as to neuropathological disorders [4]. However, the mechanisms underlying the origin and maintenance of these patterns are still largely unknown. An effective way to address these questions is through the use of animal models for which the effect of internal and external factors can be tested experimentally under controlled conditions [2,5].

A necessary first step for studying brain asymmetries is to obtain a detailed picture of normal specimens that can serve as a baseline for comparisons and thus, to recognize features that depart from expected ranges. The characterization of normal variation in the mouse brain is particularly valuable since this is the most widely used model for mammals. Even though the improvement of microMRI for small animals makes now possible to quantify multiple structures in large samples, to the best of our knowledge, only one study by Spring and collaborators [6] assessed right–left asymmetries in structures of the mouse brain using MRI. On the basis of voxel-based analyses, these authors found significant differences in size in some specific areas of the neocortex and subcortical structures.

From a methodological point of view, studies of brain structures based on MRI have mainly focused on the volumetric assessment of anatomical regions of interest (ROIs) [7–10]. This approach offers general estimations of size that are of great interest but that capture partial information of morphological traits since shape (the relative size and spatial position of traits) is also an important dimension that may vary across the brains and, therefore, requires a proper quantification [11]. Recently, Parnell and collaborators [12] have stressed the need of alternative analyses of brain morphology as they found significant shape differences in regions where volumes

* Corresponding author at: Instituto de Genética Veterinaria (IGEVET), 60 y 118 (1900) La Plata, Buenos Aires, Argentina. Tel.: +54 9 221 421 1799; fax: +54 9 221 423 6663x422.
E-mail addresses: jbarbeito@igevet.gob.ar, barbeito@fcnym.unlp.edu.ar (J. Barbeito-Andrés).

http://dx.doi.org/10.1016/j.mri.2016.04.006
0730-725X/

remained similar. In this context, geometric morphometrics based on Cartesian coordinates of points might result useful and advantageous over volumetric analyses. Geometric morphometrics combines morphometric and multivariate statistical techniques with the aim of preserving the geometry of configurations and, therefore, provides a comprehensive description of shape aspects [13]. Because within this approach shape and size can be analyzed independently, it is possible to assess whether these two morphological properties display different patterns under normal and perturbed conditions.

While geometric morphometrics has been applied to the study of different anatomical structures (especially skeletal traits), very few studies have assessed brain shape with this morphometric approach. The first applications of landmark-based analyses were carried out in samples of human brains to characterize general trends of normal morphological variation [14,15] and shape changes in the corpus callosum in human patients that had undergone fetal alcohol syndrome during their development [16,17]. In the field of paleoneurology several studies have used these morphometric toolbox to analyze hominoid endocasts, which are virtually built templates of internal neurocranial surface and are extensively used as a proxy of the brain [18–21]. More recently, landmark-based techniques have been used within a comparative framework to assess questions related to shape variation, asymmetry and modularity in humans and apes [22–24]. Nevertheless, there is still limited knowledge on the variation in shape of subcortical structures and brain shape in organisms other than humans and great apes. The availability of MRI scanners for small animals has opened a wide range of possibilities for the study of model organisms such as the mouse. However, landmark-based analyses of mouse brain shape using images obtained from MRI are still lacking (for an exception, see Sergejeva et al. [25]).

In this study, we develop a protocol that can be easily applied to images of mouse brains obtained with different combination of MRI parameters (e.g. matrix size, FOV, resolution). Specifically, we applied geometric morphometrics to point coordinates digitized on MRI to characterize normal patterns of morphological asymmetry in cortical and subcortical structures. Patterns of asymmetry were assessed in the brain as a whole as well as in eight representative substructures (cerebellum, fimbria, basal forebrain septum, olfactory bulbs, thalamus, hypothalamus, hippocampus, neocortex) by digitizing coordinates of landmarks in anatomical traits along with points that describe contours in the ROIs. These variables allow a detailed description of structural variation and provide relevant and complementary information to that obtained by volumetric and voxel-based techniques. Overall, our results will contribute to a deeper knowledge of normal variation in mouse brain, which is essential for upcoming studies that evaluate the effect of induced perturbations as deviations from a reference brain.

2. Material and methods

2.1. Sample

Brain MRIs of seven healthy adult C57BL/6J mice were obtained from MRM NeAt-Mouse Brain Dataset from the National High Magnetic Field Laboratory, FSU-UF-LANL, freely available at http://brainatlas.mbi.ufl.edu/. All specimens were male with 12 weeks of age. The analyses were performed on T2*-weight in vitro images with an isotropic resolution of 47μm, obtained with a 17.6T magnet at the University of Florida, Gainesville, FL, USA. More details about acquisition parameters are described elsewhere [26].

2.2. Morphometric data

To describe the shape of brain structures we digitized 3D coordinates of discrete anatomical points recognized at the same location in all specimens and coordinates of points describing curves (known as landmarks and semilandmarks, respectively) on selected MRI slices. Some 3D coordinates describe unpaired median traits while others correspond to paired structures at both sides of the sagittal plane.

For coordinates acquisition, first a transversal plane was defined using the flat dorsal surface of the brain as a reference. Taking into account this transversal or horizontal plane, an antero–posterior plane was defined orthogonal to the first one. This antero–posterior plane goes through the most anterior point of the left olfactory bulb (Fig. 1, right box). This antero–posterior plane is taken as a reference to define those planes where coordinates are digitized (Fig. 1, planes A–H). Planes A–H are located orthogonally to the referential antero–posterior plane and are defined in Table 1. Paxinos and Franklin atlas [27] was taken as the main reference to define the orientation of the planes of this protocol.

Landmarks and semilandmarks were digitized on A–H planes as shown in Fig. 2. By digitizing coordinates on these slices, the protocol we designed allow us to analyze not only cortical structures but also subcortical regions (e.g. hippocampus, thalamus, hypothalamus) that would be unreachable using coordinates on the outer surface of the brain. In addition, although coordinates are digitized on planes that lack themselves of three-dimensional nature, the use of several coronal slices at different locations along antero–posterior and the transversal

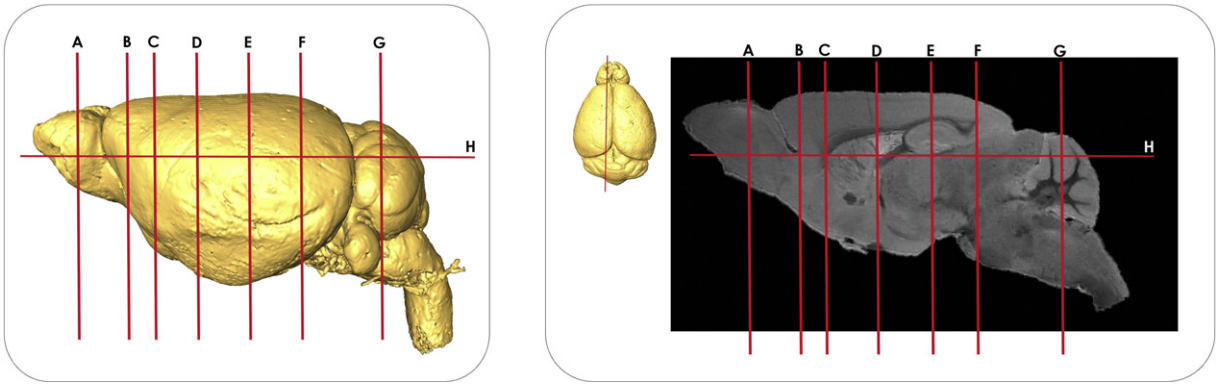

Fig. 1. Location of A–H planes used to digitize the landmarks and semilandmarks. The A–H planes are shown on the surface of the brain (left) and on the slice used as reference for defining their location (right). The slice used as reference is orthogonal to transversal and coronal planes and passes through the most anterior point of the olfactory bulbs. To define each plane, a transversal (horizontal) plane was first located on the flat dorsal surface of the brain, following Paxinos and Franklin (2001). Then, coronal planes (A–G) were defined along antero–posterior axis as orthogonal to the transversal plane and H plane was parallel to it. The definition of each plane (A–H) is available in Table 1 and the corresponding slices are shown in Fig. 2.

Table 1
Definition of planes for digitization of coordinates of landmarks and semilandmarks.

Plane	Definition*
A	Coronal middle plane in the olfactory bulbs.**
B	Coronal plane defined in the middle of between the anterior limit of the cortex and the posterior limit of olfactory bulbs.**
C	Coronal plane placed in the most anterior point of the striatum.
D	Coronal plane placed in the most anterior point of the thalamus.
E	Coronal middle plane in the hippocampus.**
F	Coronal plane placed in the most posterior point of the hippocampus.
G	Coronal middle plane in the cerebellum.**
H	Transversal plane placed just under the hippocampus.

* Planes are defined on the antero–posterior view shown in Fig. 1.
** Middle planes of brain regions are defined here by counting the number of slices and choosing the middle plane in the counting.

axes gives the opportunity to describe spatial relations between particular regions and the brain as a whole under a 3D frame.

The semilandmarks were placed along curves or contours homologous across specimens with no restriction about the correspondence of the anatomical location of each point between specimens [17]. Thus, they are especially suitable for quantifying structures with few discrete anatomical points, such as the mouse brain.

2.3. Observer repeatability

Morphometric studies are usually based on variables that are collected manually by one or different observers. Therefore, the repeatability of these measurements varies to certain degree depending on the experience of the researcher, the precision of the device used, the morphological variability of the structure under study and other conditions [28]. Evaluating whether measurements from the same set of objects are consistently obtained at different events of collection is a necessary step to validate the procedure and the resulting data.

Here, in order to estimate the repeatability in the placement of landmark coordinates on MRI slices, the set of points was digitized on the seven specimens in two events temporally spaced by two weeks. Through these analyses, it is possible to evaluate not only the repeatability in the placement of landmarks but also in the orientation and definition of the planes.

The values for each coordinate (x,y,z) in both series were compared using the intra-class correlation coefficient (ICC) [29] and repeated measure ANOVA (ANOVA-RM) [30]. The ICC is a statistical test commonly used to determine the reproducibility of a measurement. This correlation is based on variance components analysis and measures the homogeneity within groups relative to the total variation. ANOVA-MR is adequate to test the equality of means when the data violate the assumption of independence [31]. Additionally, a Euclidean or linear distance was calculated between both measurements of each landmark to obtain an estimation of the magnitude of the difference in separate events of digitization. Also, the whole sets of coordinates obtained in both series were used to perform a principal component analysis (PCA) that reduces the dimensionality of variables. After plotting the distribution of specimens of both series along main components derived from PCA, it is possible to estimate the precision in relation to sample variability [32].

Note that only the landmarks (n=130) were used to evaluate the repeatability in the digitization of coordinates. As semilandmarks do not share correspondence of the anatomical locations among specimens and they undergo a particular treatment (see Section 2.4), an assessment of congruence between events of digitization is pointless.

2.4. Assessing the magnitude and pattern of asymmetry

The configurations of landmarks and semilandmarks of all specimens were aligned to a common coordinate system by a least-squares Generalized Procrustes Analysis. This procedure translates the specimens to a common origin, scales them to unit centroid size (CS), and rotates the landmark configurations by minimizing the total sum of squared deviations of every landmark configuration from the mean configuration [33]. Because the points digitized along curves (semilandmarks) are not homologous from specimen to specimen, an extension of the standard Procrustes superimposition procedure is used to slide semilandmarks along their respective curves [17]. In addition to translating, scaling, and rotating landmarks optimally, semilandmark points are allowed to slide along their curves so as to minimize the Procrustes distance (approximated by the Euclidean distance between the sets of point coordinates) between each specimen and the average shape [17,34]. The resulting coordinates of superimposed landmarks and semilandmarks are referred to as shape coordinates as they only contain information about the shape of the configurations. Generalized Procrustes Analysis and sliding of semilandmarks were done with Morpho package in R software [35].

For structures displaying repeated traits at both sides of the sagittal plane, such as the brain and its internal sub-structures, the following procedure can be used to estimate the symmetric and asymmetric components of shape: 1) each configuration of points is reflected by reversing the signs of one of the coordinates of each landmark (x, y or z); 2) the labels of corresponding paired points are exchanged so that each paired landmark obtains the label of its counterpart; 3) the original and reflected configurations of the sample are combined and superimposed by a least-squares Procrustes analysis; 4) a symmetric component of shape of each specimen is estimated as the average between the original and reflected configuration. In this average configuration, all the unpaired landmarks fall on a plane, which is an estimate of the median plane; 5) the difference between the original and the symmetric configuration is taken as a measure of individual asymmetry [36,37]. When semilandmarks are used to describe the anatomical traits, they need to be slid before computing the asymmetric configuration in order to remove the effect of the arbitrary location in this kind of points. Here as semilandmarks were placed on separate planes, an algorithm for sliding them along their respective curves was used and they were relaxed against a perfectly symmetrized average, a procedure that takes into account the introduction of asymmetries in the process of digitizing [21,35].

Patterns of shape asymmetry were assessed by means of a two-way MANOVA on the superimposed coordinates configurations (referred to as Procrustes ANOVA) with the individual and the side as factors. In this analysis, shape variation is decomposed into variation across individuals (symmetric component), variation among right and left sides across the sample (directional asymmetry, DA) and variation due to an individual-side interaction (fluctuating asymmetry, FA). Briefly, DA represents the tendency of a morphological feature to develop differently on the right and left sides, while FA is usually interpreted as the result of random imprecisions during development that cause differences between sides [38]. When repeated measures are taken, this test also allows one to evaluate whether FA (which is usually very low) is larger than the error component, which is estimated as the residual variance.

In our data, bilateral and median coordinates were included and treated as configurations with object symmetry [37]. First, a Procrustes ANOVA on the set of landmarks (not semilandmarks) of the whole brain was carried out using the function implemented in MorphoJ 1.05, freely available at http://www.flywings.org.uk/morphoj_page.htm [39]. Then, we chose eight representative regions of the brain and assessed their asymmetry in shape by selecting those landmarks and semilandmarks that describe each of these

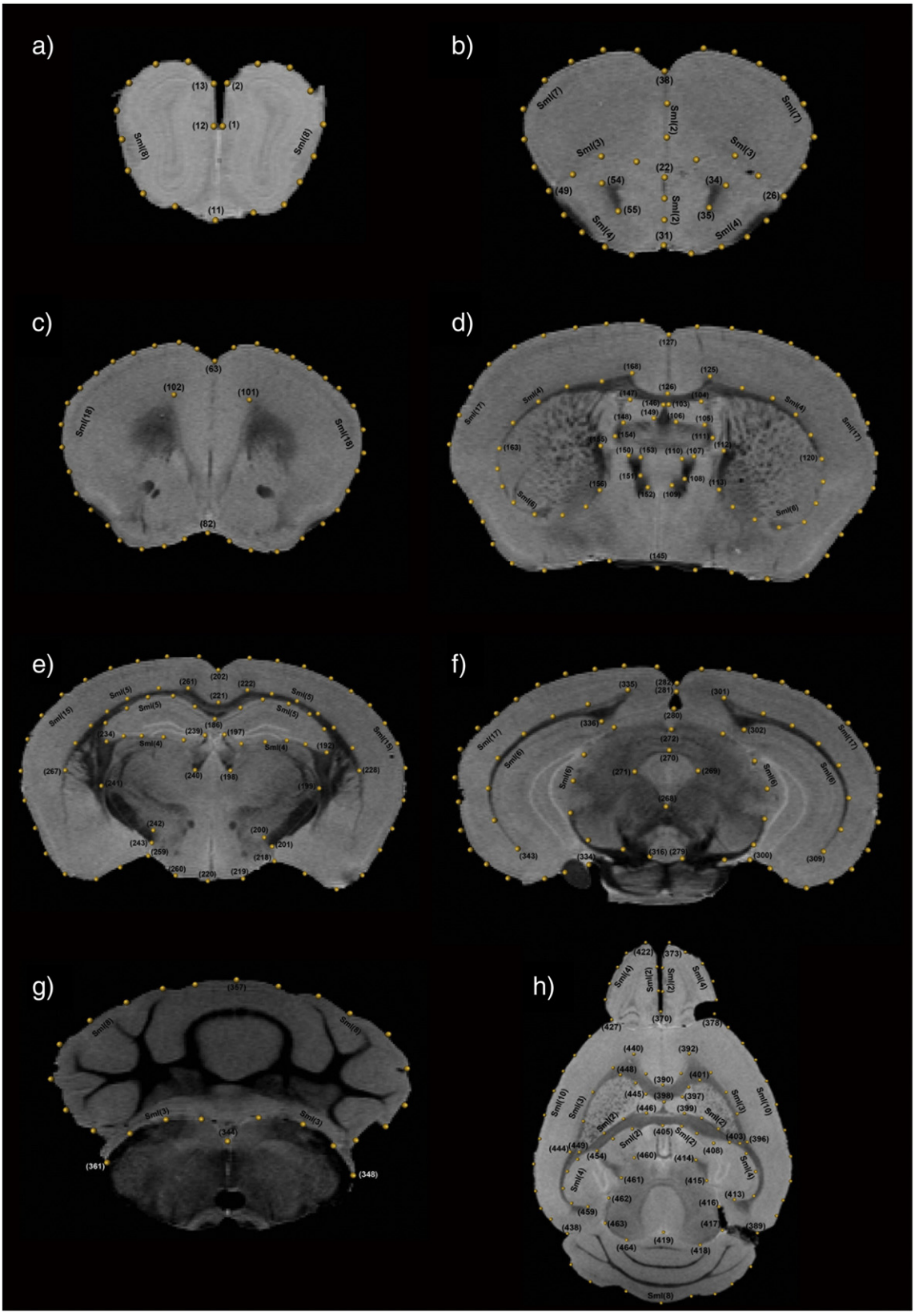

Fig. 2. Landmarks and semilandmarks digitized on A–H planes. The definition of each plane is available in Table 1.

regions (Fig. 3). Procrustes ANOVA was carried out, as explained before, on each region to assess the shape asymmetry in different brain structures using Geomorph package in R [40].

For those regions where variation due to side or individual-by-side factors resulted significant, we generated 3D visualizations to depict the patterns of location of asymmetric variation. Particularly,

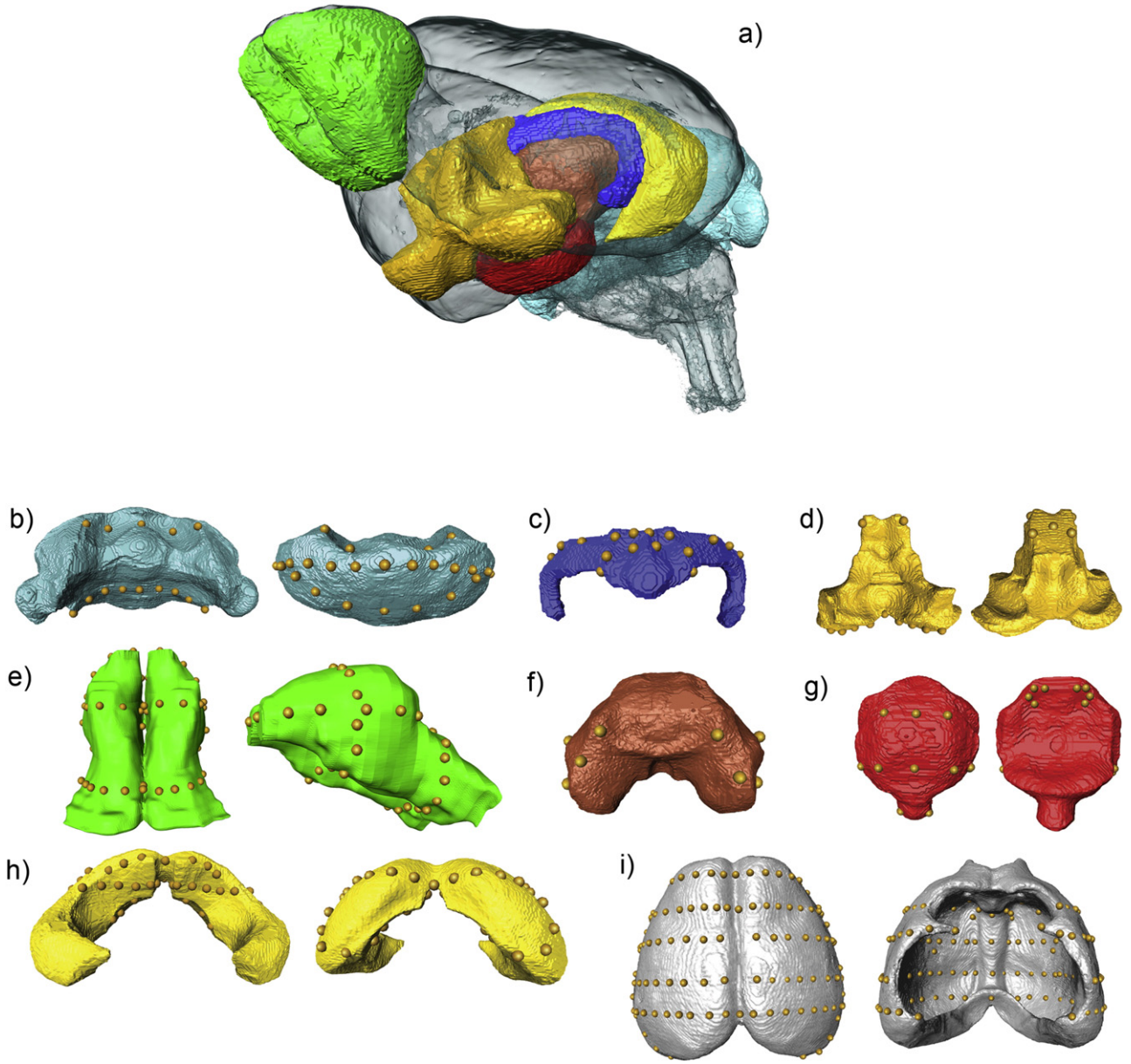

Fig. 3. 3D reconstruction of brain regions displaying the position of landmarks and semilandmarks digitized on A–H planes. Whole brain (a), cerebellum (b), fimbria (c), basal forebrain septum (d), olfactory bulbs (e), thalamus (f), hypothalamus (g), hippocampus (h) and (i) neocortex.

visualizations (colormaps) of shape changes were obtained by warping the 3D surface of each segmented region (Fig. 3) with the thin-plate spline procedure. Both original and target surfaces were kept aligned with their original axes and their differences were computed using Hausdorff distances, implemented as a filter in MeshLab (Visual Computing Lab -ISTI-CNR, http://meshlab.source.forge/). A colormap representing the differences between shapes was then constructed using the Color filter in MeshLab.

Finally, to assess size asymmetry we applied a procedure similar to the recommended for matching symmetry objects, where centroid size for right and left configurations were obtained separately and median points were not included [37]. Then, size differences between sides were evaluated through ANOVA. It is worth noting that since digitization was carried out twice, as previously explained, the average of both series for each landmark was used here.

3. Results

3.1. Observer repeatability

Analyses of observer repeatability showed that landmarks were digitized consistently at different temporal events by the same observer. Of the 130 landmarks (390 coordinates), only two coordinates displayed an F value over 5 in the ANOVA-MR and a coefficient under 0.90 in the ICC. These values, although arbitraries, can be considered as reliable points to establish which variables were measured repetitively with a large level of confidence. Additionally, linear distances between the same landmarks in both events of measurements were evaluated to show the magnitude of error. The average difference was 0.12mm, with a standard deviation of 0.05mm.

While the previous analyses (ANOVA-MR, ICC and Euclidean distances) analyzed each variable separately, PCA allowed us to

Table 2
Procrustes ANOVA of the whole brain based on the set of landmarks only.

Effect	Sum of squares	Mean Sum of squares	df	F	p (value)
Individual	0.0808556	6.61E-05	1224	10.88	<0.0001
Side	0.00222841	6.61E-05	179	2.05	<0.0001
Ind * Side	0.00652286	6.07E-06	1074	2.47	<0.0001
Error	0.00659714	2.46E-06	2681		

summarize the main trends of variation and evaluate how reliable was the digitization process at capturing these tendencies. Here, the first two PCs accounted for more than the 85% of total variation and the arrangement along these axes grouped both digitizations of the same specimens (Supplementary Fig. A1 in the online version at http://dx.doi.org/10.1016/j.mri.2016.04.006). This indicates that the ordination of specimens relative to the others was repeated in different events of measurement and observer error did not introduce an important effect when describing the most important features of shape.

3.2. Magnitude and pattern of brain asymmetry

Procrustes ANOVA of the set of landmarks that describe the whole brain indicated that both DA and FA are significant and the mean sum of squares of FA was larger than the error represented by the residuals, suggesting that it is under the magnitude we want to study and, therefore, the measurement is robust (Table 2). A visual inspection shows that particular brain regions or structures cannot be properly described using only the landmarks and in the following analyses both landmarks and semilandmarks are included (Fig. 3).

Results of Procrustes ANOVA for each brain region indicated that the greatest proportion of shape variation corresponds to the effect of differences among individuals (Table 3). Depending on the structure, approximately 61 to 87% of variation was related to the deviations of specimens' configurations to the mean, while DA usually accounted for a smaller portion of variation (between 0.820 and 12.327%) and FA ranged between 3.982 and 18.907%. Although the proportion of FA was largely smaller than variation among individuals, we found that most of the regions displayed significant FA (Table 3). In fact, except for the hypothalamus all the analyzed structures showed significant FA at a level of $p<0.0001$. For six regions (cerebellum, fimbria, basal forebrain septum, olfactory bulbs, thalamus and neocortex) DA was smaller than FA, being significant ($p<0.01$) only for the cerebellum, the fimbria, the hippocampus and the neocortex (Table 3). An overview of the results reveals that asymmetry was more evident for shape traits of the brain than for size.

Then, we obtained colormaps showing the patterns of DA and FA in those regions where variation resulted significant in the ANOVA Procrustes. Here, reddish colors represent more asymmetry and cold colors as blue are related to slight differences (Fig. 4). In the cerebellum, we found that DA is mainly localized in the posterior and dorsal region while FA is more extended and affected also the part

Table 3
Procrustes ANOVA of each region based on landmarks and semilandmarks.

Region	Effect	df	Sum of squares	Mean sum of squares	F	p (value)	% var
Cerebellum	Individual	336	0.046986	1.40E-04	11.66	1.00E-05	86.090
	Side	54	0.001638	3.03E-05	2.53	2.87E-07	3.001
	Ind * Side	324	0.003885	1.20E-05	4.46	1.00E-05	7.118
	Error	770	0.002069	2.69E-06			3.791
	total		0.054578				
Fimbria	Individual	132	0.021819	1.65E-04	3.22	0.00001	60.943
	Side	22	0.002316	1.05E-04	2.05	0.0068548	6.468
	Ind * Side	132	0.006769	5.13E-05	3.22	0.00001	18.907
	Error	308	0.004899	1.59E-05			13.682
	total		0.035803				
Basal forebrain septum	Individual	108	0.021980	2.04E-04	7.09	0.00001	75.588
	Side	17	0.000728	4.28E-05	1.49	0.112191	2.504
	Ind * Side	102	0.002926	2.87E-05	2.04	0.000004	10.062
	Error	245	0.003445	1.41E-05			11.846
	total		0.029079				
Olfactory bulbs	Individual	552	0.081220	1.47E-04	10.24	0.00001	86.689
	Side	87	0.001710	1.97E-05	1.37	0.021693	1.825
	Ind * Side	522	0.007503	1.44E-05	5.53	0.00001	8.008
	Error	1253	0.003258	2.60E-06			3.477
	total		0.093691				
Thalamus	Individual	102	0.041474	0.00040661	10.88	0.00001	81.148
	Side	18	0.000789	0.00004385	1.17	0.296419	1.544
	Ind * Side	108	0.004038	0.00003739	1.91	0.000021	7.901
	Error	245	0.004808	0.00001962			9.407
	total		0.051109				
Hypothalamus	Individual	180	0.098130	0.00054516	20.94	0.00001	86.233
	Side	29	0.000933	0.00003217	1.24	0.20358	0.820
	Ind * Side	174	0.004531	0.00002604	1.05	0.33349	3.982
	Error	413	0.010203	0.00002471			8.966
	total		0.113797				
Hippocampus	Individual	438	0.034422	7.86E-05	4.28	1.00E-05	62.641
	Side	73	0.006774	9.28E-05	5.05	1.00E-05	12.327
	Ind * Side	438	0.008046	1.84E-05	3.29	1.00E-05	14.642
	Error	1022	0.005709	5.59E-06			10.389
	total		0.054951				
Neocortex	Individual	2238	0.024076	1.08E-05	11.95	1.00E-05	85.412
	Side	364	0.000474	1.30E-06	1.45	6.37E-07	1.683
	Ind * Side	2184	0.001966	9.00E-07	2.78	1.00E-05	6.974
	Error	5159	0.001672	3.24E-07			5.931
	total		0.028188				

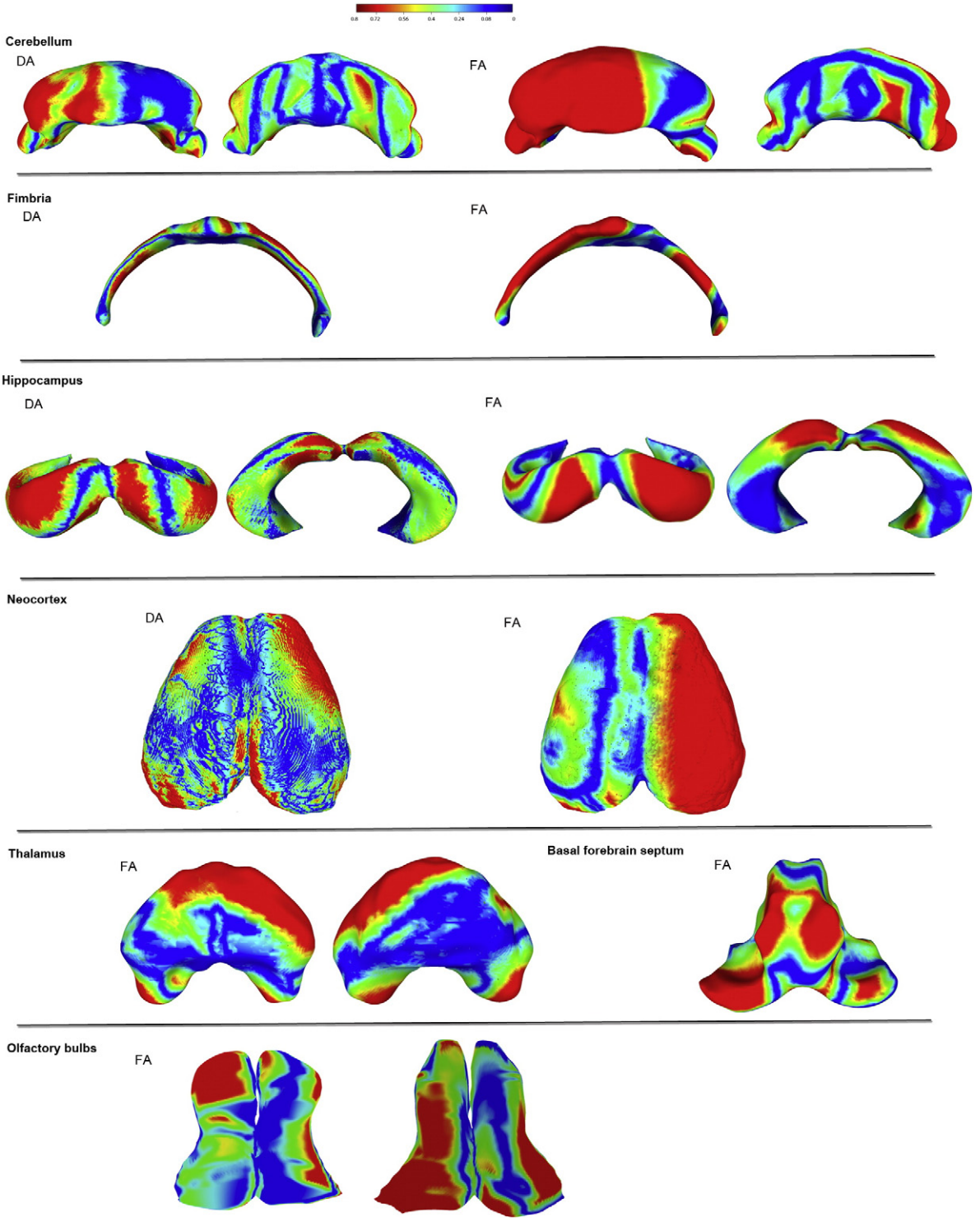

Fig. 4. DA and FA in those regions where significant variation was found. Colormaps represent the localization of asymmetric variation. The colorbar represents the magnitude of variation, starting from reddish colors for highest variation to blue for areas with the lowest asymmetry. Note that the colormaps were obtained by interpolating the shape changes captured by landmarks and semilandmarks to the entire surface, and thus, areas without points need to be interpreted with caution. Specific scale factors (SF) were empirically chosen in each region to illustrate shape variation using a magnitude that make it visible: cerebellum (SF=5), fimbria (SF=2), hippocampus (SF=2), neocortex (SF=5), thalamus (SF=2), basal forebrain septum (SF=2), olfactory bulbs (SF=5).

corresponding to the paraflocculus (ventral lateral prominences). For the fimbria, while DA is confined to some parts of the dorsal side of the branches that embrace the thalamus, FA is also present in the main body (proximal) of the fimbria showing a more widespread pattern. In the hippocampus, both DA and FA show patches indicating more asymmetry mainly in the dorsal region. For the neocortex, we found a clearly different pattern for each type of asymmetry; variation due to DA is noticeable in the most anterior extreme of the structure while FA is evident all along the antero–posterior axis. Thalamus displays FA especially in its dorsal and ventral extremes, while the middle regions seems to be unaffected by this kind of asymmetry. Main asymmetric variation can be seen in

the basal forebrain septum both in the most ventral and lateral portion of this structure and in the middle zone (main body). In the olfactory bulbs, FA is evident in the posterior extremes from a ventral position and anteriorly in the dorsal surface (Fig. 4).

Size differences between sides of each brain region are shown in Table 4. In general, all differences were subtle and only for the hippocampus the F obtained through ANOVA resulted noteworthy ($F=5.48$, $p=0.0577$). For some structures, left side was relatively larger while for others right is the predominant side, suggesting that there is no general trend for the whole brain (Table 4).

4. Discussion

In this study, we introduced a morphometric approach to assess shape and size asymmetries of the mouse brain from microMRI scans. The pipeline has the following steps: first, digitizing the coordinates of paired and unpaired landmarks and semilandmarks that describe the regions of interest on MRI slices; second, superimpose the original and reflected configurations of points of all specimens to eliminate differences in location, orientation, and standardize size; third, extract the symmetric and asymmetric components of shape variation; and finally, apply multivariate statistical analyses to assess and visualize shape asymmetry.

Besides being a reliable and repeatable procedure for landmark and semilandmark extraction, the methodological approach proposed here does not require neither spatial normalization of the MRI slices to a common space nor previous segmentation of brain structures to obtain shape data. Recently, shape asymmetries in the human brain have been assessed by using an alternative procedure that consists on segmenting structures of interest from previously normalized MRI slices, reflecting one of the sides to match the other and then quantifying differences between corresponding left–right coordinates of vertices automatically extracted [41]. The results of this procedure can be represented to display the local patterns of shape variation in the studied structures and, consequently, it is an interesting manner to mark out variation in shape asymmetry. However, geometric morphometric techniques have some advantages over these procedures because it is not necessary to count with previous normalizations and segmentations of the images. Here, we used surfaces extracted from the segmentation of specific regions only to better illustrate the results of the analyses, but data collection and analyses do not rely on surfaces derived from segmentations and the core of this methodological pipeline can be carried out without them. This is especially important since the process of segmentation can introduce error or biases in the representation of the structure, in particular when automatic and semiautomatic methods are applied instead of manual parcellation, which is taken as the "gold standard" but is known to be time consuming and expert dependent [42].

In this work, we found differences in the patterns of asymmetric variation in size and shape features in a sample of normal mouse brains. Size asymmetry was only noticeable in the hippocampus while shape asymmetries were significant in most of the studied regions. In a previous study, Spring et al. [6] found size asymmetries in restricted areas of the mouse normal brain, being the hippocampus the region with the most significant left–right differences, and they concluded that beyond some particular regions of the brain the rest of the structures cannot be considered significantly asymmetric. More recently, Parnell et al. [12] analyzed the patterns of asymmetry in volumes of different brain structures and in their shape (using an alternative method) in a mouse model of prenatal ethanol exposure and they found that shape asymmetry is significant in several regions where volumes do not display right–left differences. These findings are in line with our results, showing that size and shape asymmetries are not necessarily associated and that processes

Table 4
Centroid size differences between sides and ANOVA test for size.

Region	Difference right–left CS	Effect	Sum of squares	Mean sum of squares	df	F	p (value)	% var
Cerebellum	−0.0001881804	Individual	0.885414	0.147569	6	2.22	0.1773	68.878
		Side	0.001214	0.001214	1	0.02	0.8969	0.094
		Ind * Side	0.398846	0.066474	6	2.89	0.0478	31.027
		total	1.285474					
Fimbria	−0.0013339257	Individual	0.290060	0.048343	6	0.79	0.6074	38.236
		Side	0.102654	0.102654	1	1.68	0.2421	10.265
		Ind * Side	0.365888	0.060981	6	3.91	0.0167	48.232
		total	0.758602					
Basal forebrain septum	−0.0005600807	Individual	0.881800	0.146967	6	9.16	0.0082	87.936
		Side	0.024661	0.024661	1	1.54	0.2615	2.459
		Ind * Side	0.096319	0.016053	6	2.36	0.0867	9.605
		total	1.002780					
Olfactory bulbs	0.0015544518	Individual	4.620495	0.770083	6	8.53	0.0098	87.177
		Side	0.138241	0.138241	1	1.53	0.262	2.608
		Ind * Side	0.541406	0.090234	6	10.31	0.0002	10.215
		total	5.300142					
Thalamus	−0.0001300897	Individual	1.022474	0.170412	6	25.64	0.0005	96.026
		Side	0.002443	0.002443	1	0.37	0.5665	0.229
		Ind * Side	0.039877	0.006646	6	1.20	0.3612	3.745
		total	1.064794					
Hypothalamus	−0.0001093901	Individual	2.118148	0.353025	6	177.18	<.0001	99.407
		Side	0.000671	0.000671	1	0.34	0.5829	0.031
		Ind * Side	0.011955	0.001992	6	0.50	0.7987	0.561
		total	2.130774					
Hippocampus	3.25811565313472E-005	Individual	2.700785	0.450131	6	11.71	0.0043	85.954
		Side	0.210759	0.210759	1	5.48	0.0577	6.708
		Ind * Side	0.230569	0.038428	6	2.05	0.126	7.338
		total	3.142113					
Neocortex	5.33867299860047E-005	Individual	21.865950	3.644325	6	85.08	<.0001	98.838
		Side	0.000138	0.000138	1	0.00	0.9565	0.001
		Ind * Side	0.257013	0.042835	6	1.04	0.4405	1.162
		total	22.123101					

underlying both properties might be different. Size asymmetry is related to differences in the number or the size of cells between paired morphological structures, while shape asymmetry does not have a unidirectional link with the number and size of elemental components but would be also explained by the spatial reconfigurations of elements that change their relative position and sizes in relation to other traits. Although it is difficult to hypothesize about the functional and adaptive significance of shape asymmetry [38], our study highlights the utility of specific shape analyses going further than traditional volumetric approaches, which only account for general size differences.

The multivariate statistical methods developed for the analysis of Cartesian coordinates also allowed us to address hypotheses of shape asymmetry in the mouse brain. By means of the Procrustes ANOVA we estimated the apportionment of symmetric and asymmetric (DA and FA) variation in shape in the eight ROIs. The distribution of variation corresponding to changes among specimens and asymmetric changes displayed some differences across brain substructures (Table 4). Across all substructures DA only accounted for a modest amount of variation, ranging from 0.82% in the hypothalamus to 12.38% in the hippocampus. The limited effect of DA can be interpreted in terms of the subtle influence of those systematic developmental processes that result in differences between left and right sides. On the other hand, FA is the component of asymmetric variation that contributes the most in the eight substructures, with the highest values in the hippocampus and fimbria (almost 15 and 19%, respectively). Similar results were reported in a study of asymmetry in the external surface of the cortex of chimpanzees and humans, although the primate species displayed higher percentages of asymmetric variation than the rodent model analyzed here [23]. According to these authors, the high levels of FA that characterized primate brain can be interpreted in relation to prominent developmental plasticity, an adaptative property with important consequences in behavior and cognition. In this line, the differences in the asymmetry values between our results and the reported for primates could be thought in terms of inter-specific variation in their levels of developmental plasticity.

Beyond assessing the amount and significance of asymmetric variation, we analyzed the spatial patterns of shape asymmetry in the structures of interest. Here, visual representations of DA and FA were useful to capture differences in spatial localization of variation between both kinds of asymmetry. Therefore, the use of geometric morphometrics for brain asymmetry studies cannot only capture the effects of genetic or environmental factors but also where these effects are located.

Brain asymmetry can be of interest to very different scientific topics. In particular, experimental works with a biomedical scope may ask about the effect of different genetic, epigenetic and environmental factors on these patterns of asymmetry. It has been experimentally showed that prenatal perturbations such as maternal exposure to alcohol [12] and intrauterine growth restriction [43] might have a differential effect on both sides of the brain. In addition, several brain pathological disorders have been shown to seriously modify bilateral patterns (e.g. [41,44,45] and their accurate diagnosis may be improved if there are methodological tools that can properly distinguish between normal asymmetries and those that result from pathological conditions. In other words, it is known that mammal brain displays bilateral symmetry although it is not perfectly symmetric, and therefore the detection of perturbed patterns of asymmetry rely in a proper characterization of normal asymmetry and the comparison with sensitive methods [46]. In summary, our results based on geometric morphometrics to study normal variation in shape asymmetries of the mouse brain can serve as a starting point for future studies that address different questions of interest in neuroscience research.

Supplementary data to this article can be found online at http://dx.doi.org/10.1016/j.mri.2016.04.006.

Acknowledgements

This study was supported by grants from Consejo Nacional de Investigaciones Cientıficas y Técnicas PIP 0132 2014/2016, Agencia de Promoción Científica y Tecnológica PICT 1810 2014/2017 and Universidad Nacional de La Plata N787 2015/2018.

References

[1] Toga AW, Thompson PM. Mapping brain asymmetry. Nat Rev Neurosci 2003;4:37–48. http://dx.doi.org/10.1038/nrn1009.
[2] Halpern ME. Lateralization of the vertebrate brain: taking the side of model systems. J Neurosci 2005;25:10351–7. http://dx.doi.org/10.1523/JNEUROSCI.3439-05.2005.
[3] Habas PA, Scott JA, Roosta A, Rajagopalan V, Kim K, Rousseau F, et al. Early folding patterns and asymmetries of the normal human brain detected from in utero MRI. Cereb Cortex 2012;22:13–25. http://dx.doi.org/10.1093/cercor/bhr053.
[4] Rentería ME. Cerebral asymmetry: a quantitative, multifactorial, and plastic brain phenotype. Twin Res Hum Genet 2012;15:401–13. http://dx.doi.org/10.1017/thg.2012.13.
[5] Vallortigara G, Chiandetti C, Sovrano VA. Brain asymmetry (animal). Wiley Interdiscip Rev Cogn Sci 2011;2:146–57. http://dx.doi.org/10.1002/wcs.100.
[6] Spring S, Lerch JP, Wetzel MK, Evans AC, Henkelman RM. Cerebral asymmetries in 12-week-old C57Bl/6 J mice measured by magnetic resonance imaging. Neuroimage 2010;50:409–15. http://dx.doi.org/10.1016/j.neuroimage.2009.12.043.
[7] Kennedy DN, Lange N, Makris N, Bates J, Meyer J, Caviness VS. Gyri of the human neocortex: an MRI-based analysis of volume and variance. Cereb Cortex 1998;8:372–84.
[8] Allen JS, Damasio H, Grabowski TJ. Normal neuroanatomical variation in the human brain: an MRI-volumetric study. Am J Phys Anthropol 2002;118:341–58. http://dx.doi.org/10.1002/ajpa.10092.
[9] Mitelman SA, Brickman AM, Shihabuddin L, Newmark R, Chu KW, Buchsbaum MS. Correlations between MRI-assessed volumes of the thalamus and cortical Brodmann's areas in schizophrenia. Schizophr Res 2005;75:265–81. http://dx.doi.org/10.1016/j.schres.2004.10.014.
[10] Butler C, van Erp W, Bhaduri A, Hammers A, Heckemann R, Zeman A. Magnetic resonance volumetry reveals focal brain atrophy in transient epileptic amnesia. Epilepsy Behav 2013;28:363–9. http://dx.doi.org/10.1016/j.yebeh.2013.05.018.
[11] Adams DC, Rohlf FJ, Slice DE. Geometric morphometrics: ten years of progress following the "revolution". Ital J Zool 2004;71:5–16. http://dx.doi.org/10.1080/11250000409356545.
[12] Parnell SE, Holloway HT, O'Leary-Moore SK, Dehart DB, Paniaqua B, Oguz I, et al. Magnetic resonance microscopy-based analyses of the neuroanatomical effects of gestational day 9 ethanol exposure in mice. Neurotoxicol Teratol 2013;39:77–83. http://dx.doi.org/10.1016/j.ntt.2013.07.009.
[13] Gunz P, Mitterœcker P. Semilandmarks: a method for quantifying curves and surfaces. Hystrix Ital J Mammal 2013;24:103–9. http://dx.doi.org/10.4404/hystrix-24.1-6292.
[14] Free SL, O'Higgins P, Maudgil DD, Dryden IL, Lemieux L, Fish DR, et al. Landmark-based morphometrics of the normal adult brain using MRI. Neuroimage 2001;13:801–13. http://dx.doi.org/10.1006/nimg.2001.0748.
[15] Chollet MB, Aldridge K, Pangborn N, Weinberg SM, DeLeon VB. Landmarking the brain for geometric morphometric analysis: an error study. PLoS One 2014;9,e86005. http://dx.doi.org/10.1371/journal.pone.0086005.
[16] Bookstein FL, Sampson PD, Streissguth ANNP, Connor PD. Geometric morphometrics of corpus callosum and subcortical structures in the fetal-alcohol-affected brain. Teratology 2001;64:4–32.
[17] Bookstein FL, Streissguth AP, Sampson PD, Connor PD, Barr HM. Corpus callosum shape and neuropsychological deficits in adult males with heavy fetal alcohol exposure. Neuroimage 2002;15:233–51. http://dx.doi.org/10.1006/nimg.2001.0977.
[18] Bruner E. Geometric morphometrics and paleoneurology: brain shape evolution in the genus Homo. J Hum Evol 2004;47:279–303. http://dx.doi.org/10.1016/j.jhevol.2004.03.009.
[19] Neubauer S, Gunz P, Hublin J-J. The pattern of endocranial ontogenetic shape changes in humans. J Anat 2009;215:240–55. http://dx.doi.org/10.1111/j.1469-7580.2009.01106.x.
[20] Neubauer S, Gunz P, Hublin J-J. Endocranial shape changes during growth in chimpanzees and humans: a morphometric analysis of unique and shared aspects. J Hum Evol 2010;59:555–66. http://dx.doi.org/10.1016/j.jhevol.2010.06.011.
[21] Schlager S. Sliding semi-landmarks on symmetric structures in three dimensions. 81st Annu meet Am Assoc Phys Anthropol; 2012.
[22] Aldridge K. Patterns of differences in brain morphology in humans as compared to extant apes. J Hum Evol 2011;60:94–105. http://dx.doi.org/10.1016/j.jhevol.2010.09.007.

[23] Gómez-Robles A, Hopkins WD, Sherwood CC. Increased morphological asymmetry, evolvability and plasticity in human brain evolution. Proc R Soc Lond B Biol Sci 2013;280:20130575. http://dx.doi.org/10.1098/rspb.2013.0575.
[24] Gómez-Robles A, Hopkins WD, Sherwood CC. Modular structure facilitates mosaic evolution of the brain in chimpanzees and humans. Nat Commun 2014;5. http://dx.doi.org/10.1038/ncomms5469.
[25] Sergejeva M, Papp EA, Bakker R, Gaudnek MA, Okamura-Oho Y, Boline J, et al. Anatomical landmarks for registration of experimental image data to volumetric rodent brain atlasing templates. J Neurosci Methods 2015;240:161–9. http://dx.doi.org/10.1016/j.jneumeth.2014.11.005.
[26] Ma Y, Hof PR, Grant SC, Blackband SJ, Bennett R, Slatest L, et al. A three-dimensional digital atlas database of the adult C57BL/6 J mouse brain by magnetic resonance microscopy. Neuroscience 2005;135:1203–15. http://dx.doi.org/10.1016/j.neuroscience.2005.07.014.
[27] Paxinos G, Franklin K. The mouse brain in stereotaxic coordinates. San Diego: Academic Press; 2001.
[28] Yezerinac SM, Lougheed SC, Handford P. Measurement error and morphometric studies: statistical power and observer experience. Syst Biol 1992;41:471. http://dx.doi.org/10.2307/2992588.
[29] Shrout P, Fleiss J. Intraclass correlations: uses in assessing rater reliability. Psychol Bull 1979;2:420–8.
[30] Zar J. Biostatistical analysis. New Jersey: Prentice Hall; 1999.
[31] Lockwood CA, Lynch JM, Kimbel WH. Quantifying temporal bone morphology of great apes and humans: an approach using geometric morphometrics. J Anat 2002;201:447–64.
[32] O'Higgins P, Jones N, Facial growth in Cercocebus torquatus: an application of three-dimensional geometric morphometric techniques to the study of morphological variation. J Anat 1998;193(Pt 2):251–72.
[33] Rohlf F, Slice D. Extensions of the Procrustes method for the optimal superimposition of landmarks. Syst Biol 1990;39:40–59.
[34] Sampson P, Bookstein F, Sheehan H, Bolson E. Eigenshape analysis of left ventricular outlines from contrast ventriculograms. In: Marcus L, Corti M, Loy A, Naylor G, Slice D, editors. Adv. Morphometrics. New York, NY: Plenum; 1996. p. 131–52.
[35] Schlager S, Jefferis G. Morpho: calculations and visualisations related to geometric morphometrics; 2016.
[36] Mardia K. Statistical assessment of bilateral symmetry of shapes. Biometrika 2000;87:285–300. http://dx.doi.org/10.1093/biomet/87.2.285.
[37] Klingenberg CP, Barluenga M, Meyer A. Shape analysis of symmetric structures: quantifying variation among individuals and asymmetry. Evolution 2002;56:1909–20.
[38] Klingenberg CP, Graham JH. Analyzing fluctuating asymmetry with geometric morphometrics: concepts, methods, and applications. Symmetry (Basel) 2015;7:843–934. http://dx.doi.org/10.3390/sym7020843.
[39] Klingenberg CP. MorphoJ: an integrated software package for geometric morphometrics. Mol Ecol Resour 2011;11:353–7. http://dx.doi.org/10.1111/j.1755-0998.2010.02924.x.
[40] Adams DC, Otárola-Castillo E. Geomorph: an r package for the collection and analysis of geometric morphometric shape data. Methods Ecol Evol 2013;4:393–9. http://dx.doi.org/10.1111/2041-210X.12035.
[41] Pepe A, Zhao L, Koikkalainen J, Hietala J, Ruotsalainen U, Tohka J. Automatic statistical shape analysis of cerebral asymmetry in 3D T1-weighted magnetic resonance images at vertex-level: application to neuroleptic-naive schizophrenia. Magn Reson Imaging 2013;31:676–87. http://dx.doi.org/10.1016/j.mri.2012.10.021.
[42] Ma D, Cardoso MJ, Modat M, Powell N, Wells J, Holmes H, et al. Automatic structural parcellation of mouse brain MRI using multi-atlas label fusion. PLoS One 2014;9, e86576. http://dx.doi.org/10.1371/journal.pone.0086576.
[43] Batalle D, Munoz-Moreno E, Arbat-Plana A, Illa M, Figueras F, Eixarch E, et al. Long-term reorganization of structural brain networks in a rabbit model of intrauterine growth restriction. Neuroimage 2014;100:24–38. http://dx.doi.org/10.1016/j.neuroimage.2014.05.065.
[44] Shenton ME, Kikinis R, McCarley RW, Metcalf D, Tieman J, Jolesz FA. Application of automated MRI volumetric measurement techniques to the ventricular system in schizophrenics and normal controls. Schizophr Res 1991;5:103–13. http://dx.doi.org/10.1016/0920-9964(91)90037-R.
[45] Wahlund L-O, Andersson-Lundman G, Basun H, Almkvist O, Sparring Björkstén K, Sääf J, et al. Cognitive functions and brain structures: a quantitative study of CSF volumes on Alzheimer patients and healthy control subjects. Magn Reson Imaging 1993;11:169–74. http://dx.doi.org/10.1016/0730-725X(93)90021-5.
[46] Liu SX. Symmetry and asymmetry analysis and its implications to computer-aided diagnosis: a review of the literature. J Biomed Inform 2009;42:1056–64. http://dx.doi.org/10.1016/j.jbi.2009.07.003.